Spin-lattice coupling, frustration and magnetic order in multiferroic $RMnO_3$

X. Fabrèges[1], S. Petit[1], I. Mirebeau[1], S. Pailhès[1], L. Pinsard[2], A. Forget[3], M. T. Fernandez-Diaz[4] and F. Porcher[1]
[1] *Laboratoire Léon Brillouin, CEA-CNRS, CE-Saclay, 91191 Gif-sur-Yvette,France*
[2] *Laboratoire de Physico-Chimie de l'Etat Solide,ICMMO, Université Paris-Sud, 91405 Orsay, France*
[3] *Service de Physique de l'Etat Condensé, CEA-CNRS, CE-Saclay, 91191 Gif-Sur-Yvette, France and*
[4] *Institut Laüe Langevin, 6 rue Jules Horowitz, BP 156X, 38042 Grenoble France.*
(Dated: 01/03/2009)

We have performed high resolution neutron diffraction and inelastic neutron scattering experiments in the frustrated multiferroic hexagonal compounds $RMnO_3$ (R=Ho, Yb, Sc, Y), which provide evidence of a strong magneto-elastic coupling in the the whole family. We can correlate the atomic positions, the type of magnetic structure and the nature of the spin waves whatever the R ion and temperature. The key parameter is the position of the Mn ions in the unit cell with respect to a critical threshold of 1/3, which determines the sign of the coupling between Mn triangular planes.

Multiferroics have aroused a great attention for the last years, as the coupling between ferroelectric and magnetic orderings in these materials may open the route to novel promising electronic devices. Magnetic frustration combined with a striking magneto-elastic coupling seems to be at the origin of their properties, a cocktail that has a strong potential for novel physics[1]. These compounds are however rare, and far from being fully understood. Indeed, ferroelectricity imposes a non centrosymmetric space group [2], while magnetic frustration favors complex magnetic orders [3, 4].

The $RMnO_3$ compounds, where R is a rare earth ion, follow these conditions. In orthorhombic $RMnO_3$, (R=Eu, Gd, Tb, Dy), where the strong $GdFeO_3$-type distortion lifts the orbital degeneracy, magnetic frustration arises from competing super-exchange interactions [5], yielding incommensurate magnetic structures [6]. This peculiar ordering suggested a novel coupling between dielectric and magnetic collective modes [7]. In hexagonal $RMnO_3$ with smaller R ionic radius, (R=Ho, Er, Yb, Lu, Y), magnetic frustration arises from the triangular geometry [8], yielding 120° Néel orders for the Mn moments [9]. In $YMnO_3$ and $LuMnO_3$, where Y and Lu are non magnetic, an iso-structural transition was recently observed at the Néel temperature T_N [10], namely each ion "moves" inside the unit cell when Mn moments get ordered. This effect provided evidence for a giant magneto-elastic coupling, likely connected with an increase of the ferroelectric polarization [11]. Its origin remains unexplained so far.

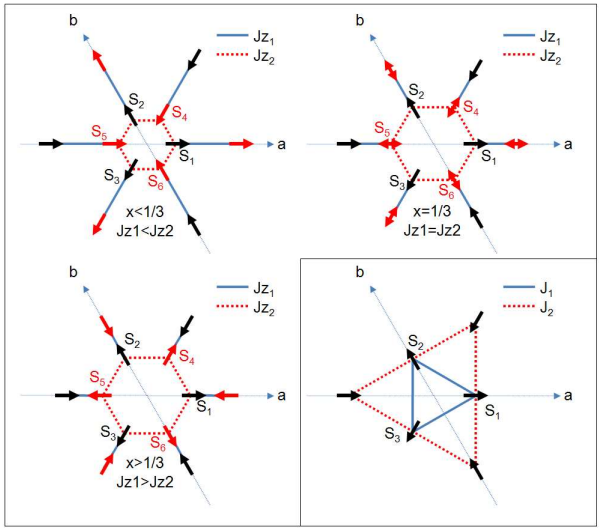

FIG. 1: [Colors on line]. Sketch of the hexagonal MnO planes with out-of-plane exchange paths J_{z1} (between $\vec{S}_4$ and $\vec{S}_3$) and J_{z2} (between $\vec{S}_4$ and $\vec{S}_1$ as well as $\vec{S}_4$ and $\vec{S}_2$). Black (red) arrows depict the positions of the Mn spins within z=0 (z=1/2) Mn planes. $\vec{S}_1, \vec{S}_2$ and $\vec{S}_3$ are located at $(x,0,0)$, $(0,x,0)$, $(-x,-x,0)$, while $\vec{S}_4, \vec{S}_5, \vec{S}_6$ at $(x,x,1/2)$, $(1-x,0,1/2)$ and $(0,1-x,1/2)$. Double arrows are used when several spin orientations can be stabilized. Inset : sketch of the hexagonal MnO plane with in-plane exchange paths J_1 and J_2.

To shed light on these materials, we carried out high resolution neutron diffraction and inelastic neutron scattering in four $RMnO_3$ (R=Y, Sc, Ho, Yb), with either non magnetic (Y, Sc) or magnetic (Ho, Yb) R ion, showing (Ho, Sc) or not (Y,Yb) a spin reorientation at T_{SR} with temperature [12, 13, 14]. We show that the iso-structural transition is a systematic feature in the hexagonal series. In addition, we establish a correlation between the atomic positions, the type of magnetic structure, and the nature of the spin waves, whatever the compound and its magnetic structure. We show that the key parameter is the position x of the Mn ions within the triangular plane with respect to a critical threshold of 1/3 which tunes the sign of the interplane exchange interaction. We justify this result by simple energy arguments. Thanks to the magneto-elastic coupling, the atomic motion helps releasing the frustration by selecting a given magnetic structure, depending on the x value. This process recalls the spin-Peierls states stabilized in several geometrically frustrated 2D or 3D compounds [15, 16].

Hexagonal $RMnO_3$ compounds consist of stacked Mn-O and R layers, the Mn ions forming a nearly ideal two dimensional triangular lattice [17]. They crystallize in the $P6_3cm$ space group, with two Mn-O planes per unit cell. As shown on Figure 1, Mn coordinates depend on a unique parameter x. For $x \neq 1/3$, two different exchange path J_1 and J_2 can be defined between Mn moments in a given Mn plane (inset Fig. 1). The triangular symmetry and hence the geometrical frustration within a Mn plane is however preserved whatever the x value. The Mn-Mn interactions between adjacent Mn planes are due to super-super exchange paths, via the apical oxygen ions of MnO_5 bipyramids. These interactions lead to a 3D magnetic ordering below T_N. Again, as soon as $x \neq 1/3$, two different paths, and thus two different interactions, J_{z1} and J_{z2}, can be distinguished (Fig.1), while for $x = 1/3$ all paths become equivalent. The value $x = 1/3$ is therefore a critical threshold which determines the sign of the effective interplane exchange $J_{z1} - J_{z2}$ (the same sign as that of $x - 1/3$). As shown below, this quantity determines in turn the stability of the magnetic phases and the nature of the spin waves.

Whatever the x value and the R magnetism, the Mn magnetic moments order in 120° arrangements, with four different possible structures (inset Fig. 2), labeled from the irreducible representations (IR) $\Gamma_{i,\ i=1-4}$ of the $P6_3cm$ space group with $\mathbf{k}$=0 propagation vector [12, 18]. For Γ_1 and Γ_4, Mn moments are perpendicular to a and b axes, and their arrangement in the $z = 1/2$ plane are either antiparallel (Γ_1) or parallel (Γ_4) with respect to z=0. The same picture holds for Γ_2 and Γ_3 with spins along a and b axes.

High-resolution neutron powder diffraction patterns were collected versus temperature on the D2B and 3T2 instruments, at ILL and LLB-Orphée reactors respectively. Powder samples $HoMnO_3$, $ScMnO_3$ and $YbMnO_3$ were prepared as described in [19] and characterized by x-ray diffraction. Data were analyzed using the Fullprof and Basireps softwares [20, 21], allowing us to determine the atomic positions and the magnetic structures versus temperature precisely. The magnetic structures and transition temperatures agree with previous determinations [9, 12]. It is worth noting that $HoMnO_3$ and $ScMnO_3$ undergo a second magnetic transition at T_{SR} corresponding to the reorientation of the Mn spins.

Figure 2 shows the temperature dependence of the Mn position x for the three samples. As a striking feature, in $HoMnO_3$, x exhibits an unprecedented large change (of about 3%), which occurs at T_N, providing evidence for an iso-structural transition concomitant with the magnetic ordering. Smaller changes occur at T_N in $ScMnO_3$ and $YbMnO_3$. These results confirm those previously obtained [10] in Y and $LuMnO_3$, and show that this transition is universal in the hexagonal $RMnO_3$ series. As noticed in Ref.10, the variations of x versus T depend of the rare-earth ion, namely x increases below T_N in Ho

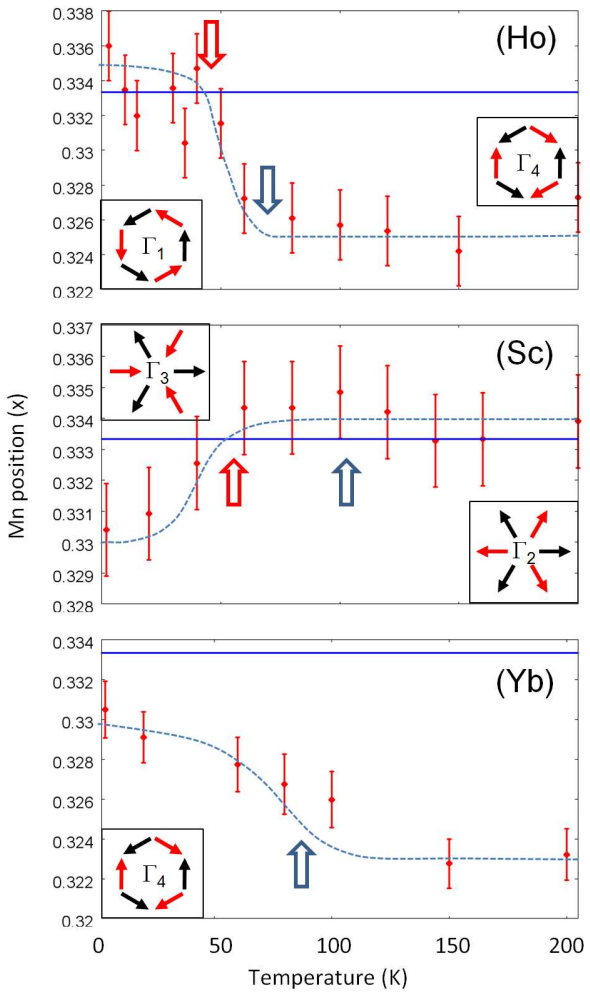

FIG. 2: [Color online]. Refined Mn positions in the unit cell obtained from high-resolution neutron powder diffraction. Blue and red arrows indicate respectivly the Néel and the spin reorientation temperatures. Lines are guides to the eyes. Right insets : Mn magnetic configuration for $T_{SR} < T < T_N$. Left insets : Mn magnetic configuration $T < T_{SR}$).

and $YbMnO_3$, whereas it decreases in $ScMnO_3$. Moreover, we also discern important changes at the reorientation transition. In $HoMnO_3$, x increases with decreasing temperature and crosses the 1/3 threshold exactly at the spin reorientation temperature (T_{SR}). The reverse situation holds for $ScMnO_3$, where x decreases upon cooling, becoming lower than 1/3 at T_{SR}. Finally, in $YbMnO_3$, which shows no reorientation transition, x increases at T_N but remains lower than 1/3 in the whole temperature range.

All these features can be explained by considering the strategic position of the Mn ions. We argue that x is the key parameter that controls the sign of $J_{z1} - J_{z2}$ and thus drives the magnetic ordering. Namely for $x \leq 1/3$, the exchange path along J_{z1} is longer than along J_{z2} and we expect $J_{z1} - J_{z2} \leq 0$. The reverse situation

R ion	IR		Positions	
	T_N	1.5K	T_N	1.5K
Yb	Γ_4	Γ_4	0.3270(15)	0.3310(14)
Ho	Γ_4	Γ_1	0.3261(21)	0.3359(19)
Sc	Γ_2	Γ_3	0.3342(18)	0.3304(17)
Y	Γ_1	Γ_1	0.3330(17)	0.3423(13)

TABLE I: Mn position in $RMnO_3$ compounds correlated with their magnetic structures defined by Γ irreducible representations. $YMnO_3$ positions are taken from Ref. 10

occurs for $x \geq 1/3$. A careful look at the positions and magnetic structures summarized in table I shows that $x \leq 1/3$ is associated with Γ_3 and Γ_4 while $x \geq 1/3$ corresponds to Γ_1 and Γ_2. This scheme also explains the occurrence of a spin reorientation transition when x crosses the 1/3 threshold. In this case, $J_{z1} - J_{z2}$ changes sign, resulting in a change from Γ_1 towards Γ_4 (Ho) or from Γ_2 towards Γ_3 (Sc). The crucial importance of the $J_{z1} - J_{z2}$ coupling can be further justified by calculating the magnetic energy $\mathcal{E}$ (per unit cell) of the Mn moments in a mean field approximation. $\mathcal{E}$ is readely obtained by writting the Heisenberg Hamiltonian : $\mathcal{H} = \mathcal{H}_p + \mathcal{H}_z$, with $\mathcal{H}_p = \sum J\ \vec{S}_i\vec{S}_j$, and $\mathcal{H}_z = \sum J_z\ \vec{S}_i\vec{S}_j$, where the sums run over nearest neighbors and the subscripts p and z refer to in plane and out of plane interactions respectively. Because of the triangular arrangement, we have $\sum_{i=1,2,3} \vec{S}_i = \sum_{i=4,5,6} \vec{S}_i = 0$, which in turn implies : $\mathcal{E} = -\frac{3}{2}JS^2 + (J_{z1} - J_{z2})(\vec{S}_3.\vec{S}_4)$. Depending on its sign, parallel or antiparallel orientations of $\vec{S}_3$ and $\vec{S}_4$ are expected, giving rise to the four magnetic structures described above. Within this simple picture, Γ_1 and Γ_2 IR minimize the energy for $J_{z1} - J_{z2} \geq 0$ while Γ_3 and Γ_4 are favored for $J_{z1} - J_{z2} \leq 0$. This is in exact agreement with the results summarized in Table 1.

A straightforward way to confirm our explanation is to determine the value of $J_{z1} - J_{z2}$ by an independent measurement. This can be easely done by measuring the spin wave dispersion along the c-axis. For this purpose we carried out inelastic neutron scattering experiments on the cold triple-axis 4F spectrometer installed at LLB-Orphée, on large single crystals of $YMnO_3$, $YbMnO_3$ and $HoMnO_3$ grown by the floating zone technique.

Figure 3(left) shows a color map of the dynamical structure factor measured as a function of energy and wavevector in $YMnO_3$, $YbMnO_3$ and $HoMnO_3$. These maps were obtained by collecting energy scans taken at different $(1, 0, Q_\ell)$ wavevectors. The measurements were performed at 2 K in the first two cases, and at two temperatures just above and below the re-orientation temperature T_{SR} for $HoMnO_3$. Different features can be seen from these experimental data, including crystal field levels (Yb and Ho). A comprehensive investigation of of these features is however beyond the scope of this paper and we would like to focus on the low energy spin wave excitations labelled with arrows. We notice that in $YMnO_3$ and $YbMnO_3$, this particular branch displays upwards (Yb) or downwards (Y) dispersions, revealing opposite couplings along c. Similarly in $HoMnO_3$, when crossing the reorientation T_{SR}, the curvature changes from upwards to downwards, indicating a reversal of the magnetic interaction along the c-axis.

To get a quantitative information about these couplings, we performed a spin wave analysis of the Heisenberg Hamiltonian $\mathcal{H} = \mathcal{H}_p + \mathcal{H}_z$ defined above, taking into account additional planar and uniaxial anisotropy terms [22, 26]. Figure 3(right) shows the dynamical structure factors calculated on the basis of this model as a function of energy transfer ω and wavevector $(1, 0, Q_\ell)$. In this approach, six spin wave modes are expected. Along c, four of them are almost degenerate. They exhibit a large gap due to the planar anisotropy, as well as a very weak dispersion. On Figure 3 (right), these modes correspond to the flat branch sitting at 5 meV (Ho,Y) or 6 meV (Yb). The two remaining modes correspond to the Goldstone modes of the magnetic structure. In $q = 0$ limit, they can be seen as global rotations of the 120° pattern inside the basal planes. They couple via the J_z interactions, resulting in either in phase or out of phase rotations. These two modes are pointed out by arrows in Figure 3 (right). Actually, one of them has a vanishing intensity but can still be observed around (101). Assuming antiferromagnetic couplings J_{z1} and J_{z2}, we can determine from the data $J_{z1} - J_{z2} = 0.0050(5)$ meV in $YMnO_3$ and $J_{z1} - J_{z2} = -0.012(2)$ meV in $YbMnO_3$. For $HoMnO_3$, the neutron data are well modelled with $J_{z1} - J_{z2} = -0.0038(5)$ meV at T=45K $\geq T_{SR}$ and with $J_{z1} - J_{z2} = 0.0018(5)$ meV at T=27K $\leq T_{SR}$. We note that the corresponding signs of $J_{z1} - J_{z2}$ deduced from these measurements are fully consistent with the diffraction analysis.

Our analysis emphasizes the double origin of the magnetic frustration. The Mn triangular planes are geometrically frustrated for antiferromagnetic interactions. In addition, adjacent Mn planes are coupled along the c axis by self-competing interactions. The Mn shift with respect to the 1/3 position does not suppress the rotational invariance in the Mn plane, but clearly lifts the interplane frustration, allowing 3D ordering. Depending on x, either (Γ_1, Γ_2) or (Γ_3, Γ_4) structures are stabilized. The remaining degree of freedom in the system is the global rotation of a 120° Néel order around the c-axis. Namely, to stabilize Γ_1 or Γ_2 (Γ_3 or Γ_4), the Mn magnetic moments must couple to the (a, b) crystal axes.

On the one hand, residual anisotropic interactions among Mn ions can in principle select a given orientation in a Mn plane. As revealed by the exceptionally small uniaxial gap observed in $YMnO_3$ [22, 26], these interactions are weak. They are not sufficient to break the triangular symmetry, so that two-dimensional spin liquid fluctuations remain [22]. On the other hand, one could argue that R-Mn interactions (when R is magnetic) play

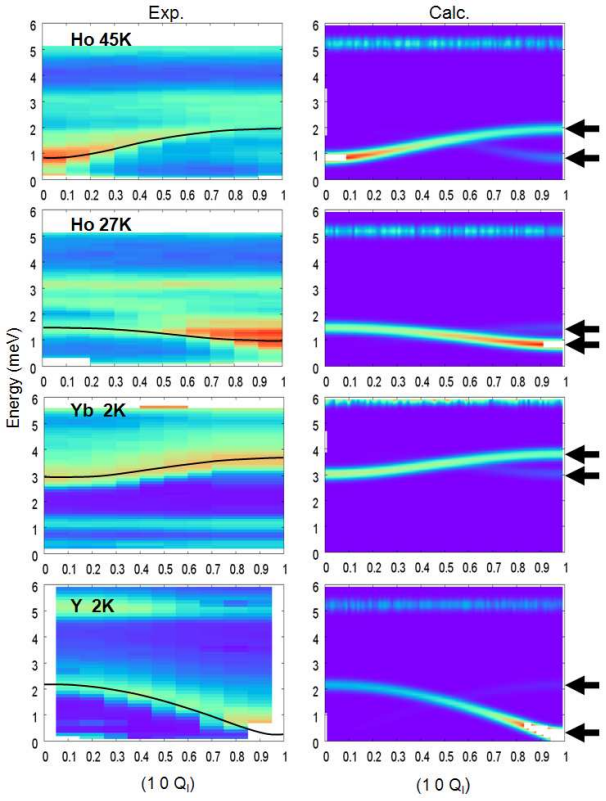

FIG. 3: (color online.) Maps of the dynamical structure factor in Ho, Yb and $YMnO_3$. The neutron intensity is plotted versus the energy transfer ω and wave vector $(1, 0, Q_\ell)$. Left panel : experimental results from inelastic neutron scattering. Black lines highlight the low energy spin wave modes. Additional Q-independent lines in Yb and $HoMnO_3$ maps are due to crystal field excitations. Right panel : spin wave dispersion curves calculated using an Heisenberg Hamiltonian. Black arrows indicate the two Goldstone modes (see text).

a significant role. Indeed, the R moments on the $4b$ site order at T_N in the Mn molecular field, while their orientations are clearly coupled to the Mn ones, through an energy term of anisotropic nature [14]. Our spin wave measurements (Fig 3) show that the uniaxial anisotropy gap in $YbMnO_3$ (3 meV) varies with temperature like the Yb moment, providing evidence for such R-Mn coupling. Nevertheless, we shall not conclude that the Mn orientation in the (a, b) plane is completely determined by this interaction. For instance, spin reorientation transitions of the Mn sublattice may occur (Sc, Ho) or not (Y, Yb) whatever the R magnetism.

In conclusion, our elastic and inelastic neutron scattering experiments clearly show the crucial role of the Mn position in determining both the magnetic structure and the spin waves modes. The onset of Mn magnetic orderings at T_N or T_{SR} correlates with the Mn position. The magnetic orders and spin excitations in the whole series result from a subtle interplay of magneto-elastic coupling, frustrated intra- and inter-plane Mn-Mn interactions and R-Mn interactions. The strong importance of inter-plane interactions strongly suggests that the shift of the Mn position, which releases the frustration along the c axis, is a key ingredient at the origin of the multiferroicity in the hexagonal $RMnO_3$ family. We thank E. Suard for her help in the D2B experiment and V. Simonet and F. Damay-Rowe for useful discussions.

[1] S-W Cheong, M. Mostovoy, Nature Materials **6**, 13 (2007).
[2] M. Fiebig, J. Phys. D: Appl. Phys. **38**, R 123 (2005).
[3] J. E. Greedan J. Mater. Chem. **11**, 37 (2001).
[4] R. Moessner and A. P. Ramirez Physics Today **59**, 24 (2006).
[5] T. Kimura *et al.*, Phys. Rev. B **68**, 060403(R) (2003).
[6] M. Kenzelmann *et al.* Phys. Rev. Lett. **95**, 087206 (2005).
[7] H. Katsura, A. V. Balatsky and N. Nagaosa Phys. Rev. Lett. **98**, 027203 (2007).
[8] Th. Jolicoeur, J. C. Le Guillou, Phys. Rev. B **40**, 2727 (1989).
[9] A. Munoz *et al.*, Chem. Mater., **13**, 1497-1505 (2001).
[10] S. Lee *et al.* Nature **451**,805 (2008).
[11] S. Lee *et al.* Phys. Rev. B **71** 180413(R) (2005)
[12] A. Munoz *et al.*, Phys. Rev. B, **62**, 9498 (2000).
[13] P. J. Brown and T. Chatterji, J. Phys. Cond. matter, **18**, 10085-10096 (2006).
[14] X. Fabrèges *et al.* Phys. Rev. B, **78**, 214422 (2008).
[15] F. Becca and F. Mila Phys. Rev. Lett., **89**, 037204 (2002).
[16] O. Tchernyshyov, R. Moessner and S. L. Sondhi Phys. Rev. Lett., **88**, 067203 (2002).
[17] T. Katsufuji *et al.*, Phys. Rev. **B 66**, 134434 (2002).
[18] E. F. Bertaut, C. R. A. S. **252**,76 (1961).
[19] J. A. Alonso, M.J. Martinez-Lope, M.T. Casais, M.T. Fernandez-Diaz, Inorg. Chemistry, **39**, 917-923 (2000).
[20] J. Rodriguez-Carvajal, Physica B, **192**, 55-69 (1993)
[21] J. Rodriguez-Carvajal, http://www.ill.eu/sites/fullprof/php/program
[22] T.J. Sato *et al.*, Phys. Rev. B **68**, 014432 (2003).
[23] J. Park *et al.* Phys. Rev. B **68**, 104426 (2003).
[24] O.P. Vajk, M. Kenzelmann, J. W. Lynn, S. B. Kim, S.-W. Cheong, Phys. Rev. Lett. **94**, 087601 (2005).
[25] T. Chatterji, S. Ghosh, A. Singh, L. P. Régnault and M. Rheinstadter, Phys. Rev. B **76**, 144406 (2007).
[26] S. Petit *et al.*, Phys. Rev. Lett. **99**, 266604 (2007).
[27] S. Pailhès *et al.*, Phys. Rev. B **79**, 134409 (2009).